Unifying disparate experimental views on shear-thickening suspensions

Preprint · January 2020

CITATIONS
0

READS
300

5 authors, including:

Philippe Bourrianne
ESPCI Paris
24 PUBLICATIONS **300** CITATIONS
SEE PROFILE

Thibaut Divoux
Ecole normale supérieure de Lyon
114 PUBLICATIONS **2,990** CITATIONS
SEE PROFILE

Gareth H. McKinley
Massachusetts Institute of Technology
544 PUBLICATIONS **36,610** CITATIONS
SEE PROFILE

Unifying disparate experimental views on shear-thickening suspensions

Philippe Bourrianne,[1] Vincent Niggel,[1] Gatien Polly,[1,2] Thibaut Divoux,[2,3] and Gareth H. McKinley[1]

[1] *Hatsopoulos Microfluids Laboratory, Department of Mechanical Engineering, MIT, 77 Massachusetts Avenue, Cambridge, MA 02139, USA*
[2] *MultiScale Material Science for Energy and Environment, UMI 3466, CNRS-MIT, 77 Massachusetts Avenue, Cambridge, MA 02139, USA*
[3] *Department of Civil and Environmental Engineering, MIT, 77 Massachusetts Avenue, Cambridge, MA 02139*

(Dated: January 9, 2020)

Shear thickening denotes the rapid and reversible increase in viscosity of a suspension of rigid particles under external shear. This ubiquitous phenomenon has been documented in a broad variety of multiphase particulate systems, while its microscopic origin has been successively attributed to hydrodynamic interactions and frictional contact between particles. The relative contribution of these two phenomena to the magnitude of shear thickening is still highly debated and we report here a discriminating experimental study using a model shear-thickening suspension that allows us to tune independently both the surface chemistry and the surface roughness of the particles. We show here that both properties matter when it comes to continuous shear thickening (CST) and that the presence of hydrogen bonds between the particles is essential to achieve discontinuous shear thickening (DST) by enhancing solid friction between closely contacting particles. Moreover, a simple argument allows us to predict the onset of CST, which for these highly-textured particles occurs at a critical volume fraction much lower than that previously reported in the literature. Finally, we demonstrate how mixtures of particles with opposing surface chemistry make it possible to finely tune the shear-thickening response of the suspension at a fixed volume fraction, paving the way for a fine control of shear-thickening transition in engineering applications.

Suspensions composed of rigid particles dispersed in a liquid matrix are ubiquitous in daily life, from cosmetics and consumer products (e.g., tooth paste) to foodstuffs (e.g., coffee) and engineering materials such as fresh cement paste. Their flow properties display a broad variety of rheological behavior depending on the volume fraction ϕ and the nature of the physico-chemical interactions between particles [1, 2]. In the semi-dilute regime, suspensions show a shear-thinning response, i.e., their shear viscosity η decreases for increasing applied shear rate $\dot{\gamma}$. Such behavior, which results from long-range hydrodynamic interactions and possible shear-induced structure formation [3–6], is amplified in the presence of attractive interactions between particles, which at moderately high volume fraction eventually confer a yield stress to the suspension, i.e., the material becomes paste-like with a solid-like elasto-plastic behavior at rest [7].

Conversely, so-called "dense suspensions" (i.e., suspensions with high volume fraction) exhibit shear thinning under weak shearing conditions followed by a shear-thickening transition for large enough shear, defined by a rapid and reversible increase of viscosity with the shear rate, or shear stress [8–10]. The magnitude of the shear thickening is enhanced by increasing the volume fraction. At intermediate volume fractions, continuous shear thickening (CST) ranges from a mild increase in viscosity that was initially explained by lubricated hard-sphere interactions [11, 12] to a more pronounced effect when particle interactions involve frictional contacts [13]. Finally, for very large volume fractions, closer to the jamming volume fraction ϕ_J [14], the viscosity may jump by orders of magnitude at constant shear rate [15, 16]. Such a discontinuous shear thickening (DST) response was first associated with the formation of "hydroclusters" [17–21], before being attributed primarily to frictional interactions [13, 15, 22–27] or even shear-jamming regimes [28], while the bulk suspension remains homogeneously sheared in that regime [29]. The nature of local inter-particle interactions, mediated by the suspending solvent, affects this picture. Indeed, the shear-thickening transition is enhanced when particles show moderate attraction [30], and suppressed in presence of strong short-range inter-particle attractions due to the presence of a yield stress [31, 32]. More recently, hydrogen bonding interactions were shown to enhance DST by favoring weak and reversible adhesion between particles [24, 33–35].

As of now, DST has, in general, been associated with dense suspensions, i.e., for ϕ relatively close to the jamming fraction ϕ_J [27, 36, 37]. In this framework, the current mechanistic interpretation of DST relies on the divergence of the suspension viscosity in the vicinity of ϕ_J [15]. The relative contributions of the solid friction and the chemical interactions at the molecular scale to the magnitude and dynamic of the DST remain to be quantified, but are embodied qualitatively in the magnitude of the friction coefficient between particles. Here we report an experimental study on suspensions of colloidal fumed silica particles suspended in a viscous oligomeric polar solvent. We show that these suspensions, which do not exhibit any ageing, drying, migration or settling (in sharp contrast to cornstarch or other non-Brownian suspensions) can display both CST and DST transitions

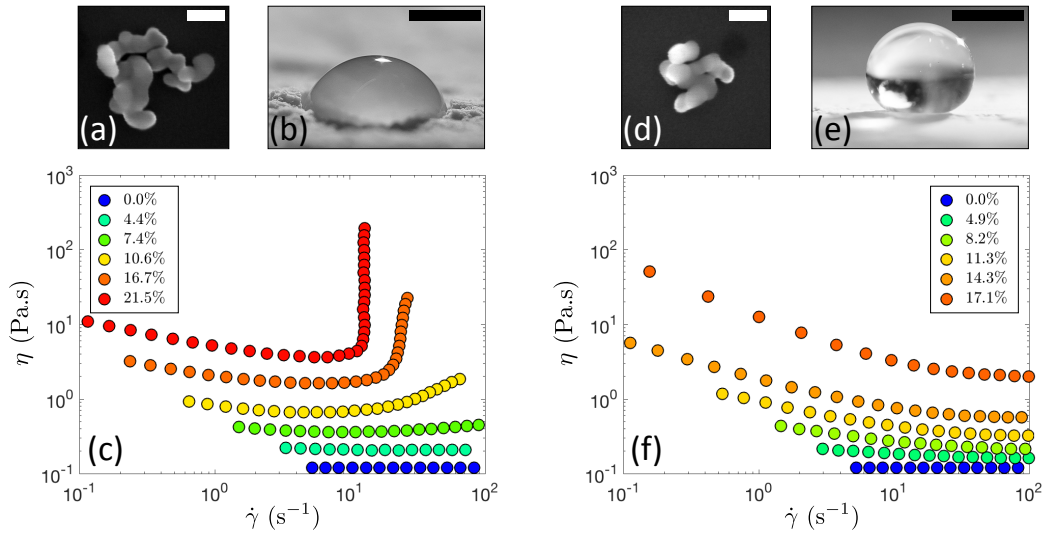

FIG. 1: (color online) (a) Scanning Electron Microscopy (SEM) images of a hydrophilic fumed silica particle. The scale bar represents 100 nm. (b) Hydrophilic fumed silica particles coated on a glass slide are wetted by a drop of water due to their hydrophilic nature. The scale bar is 1 mm. (c) Flow curves $\eta(\dot{\gamma})$ measured for suspensions of hydrophilic fumed silica particles at various volume fractions $0 \leq \phi \leq 21.5\%$. The suspensions of hydrophilic particles show successively CST, and then DST, for increasing ϕ. (d) SEM picture of a hydrophobic fumed silica particle. The scale bar represents 100 nm. (e) A water drop is repelled by a coating made by depositing a layer of hydrophobic fumed silica particles on a glass slide. The superhydrophobic character of the coating highlights the hydrophobic chemistry of the particles. The scale bar represents 1 mm. (f) Viscosity η of a suspension of hydrophobic fumed silica as a function of shear rate $\dot{\gamma}$ at various volume fractions ϕ. The suspensions of hydrophobic particles display a shear-thinning response for all the volume fractions tested.

at much lower volume fractions than values traditionally reported in the literature. Furthermore, these particles allow us to tune independently their surface chemistry and their effective surface roughness, which makes it possible to identify the relative contributions of both friction and reversible chemical adhesion to the shear-thickening transition. We demonstrate that removing frictional interactions fully suppresses the shear-thickening transition. Finally, by mixing hydrophilic and hydrophobic particles in varying fractions, we study the competition between initiation and inhibition of the discontinuous shear-thickening transition, which allows us to smoothly tune the onset and extent of DST.

To study the shear thickening transition we utilize four distinct fumed silica systems that enable us to vary both the roughness and the hydrophilicity of the particles while holding the average particle size constant at $D \simeq 300$ nm. These textured fumed silica particles are composed of nodules of size R_u that are fused together permanently during the flame synthesis [38]. The sintered aggregates confer nanometric textures and high specific areas to the particles [see Fig. 1(a) and SI-1]. We consider here two classes of fumed silica particles which differ by the size R_u of the primary unit and consequently by their nanometric roughness. A smaller primary unit ($R_u = 10$ nm, later denoted as "rough" fumed silica) induces rougher textures (i.e., higher specific area) than larger nodules ($R_u = 25$ nm, "smooth" fumed silica). Both of these types of particles are naturally strongly hydrophilic due to both the presence of surface hydroxyl groups and to their intrinsic submicronic roughness as seen in the picture in Fig. 1(b). When dispersed in polypropylene glycol (PPG, $\eta_0 = 120$ mPa.s, $M_w = 725$ g/mol), i.e., a polar solvent, fumed silica particles display a stabilizing solvation layer that prevents irreversible aggregation [39]. The resulting suspensions are transparent and show excellent stability over time with no thixotropy or ageing (see SI-2). We have prepared suspensions at various volume fractions ϕ by varying the mass ratio of particles dispersed. The true volume fraction of the particulate phase is carefully determined by performing precise density measurements of the suspension (see SI-3). Finally, the steady rheological response of the suspensions is measured by a slowly decreasing ramp of shear stress imposed in a cone and plate geometry connected to a stress-controlled rheometer (see SI-4).

The rheometric response of "smooth" ($R_u = 25$ nm) hydrophilic fumed-silica suspensions is reported in Fig. 1(c) for volume fractions ranging between $\phi = 0\%$ and 21.5%. Increasing the mass of dispersed particles leads to a departure from the Newtonian response of the pure solvent ($\eta_0 = 120$ mPa.s). At low volume fractions, the suspension shows a weakly shear-thinning behavior characterized by a slow decrease of the viscosity η for increasing shear rates $\dot{\gamma}$. At intermediate volume fractions ($\phi \simeq 7.4\%$), the shear-thinning behavior persists at low

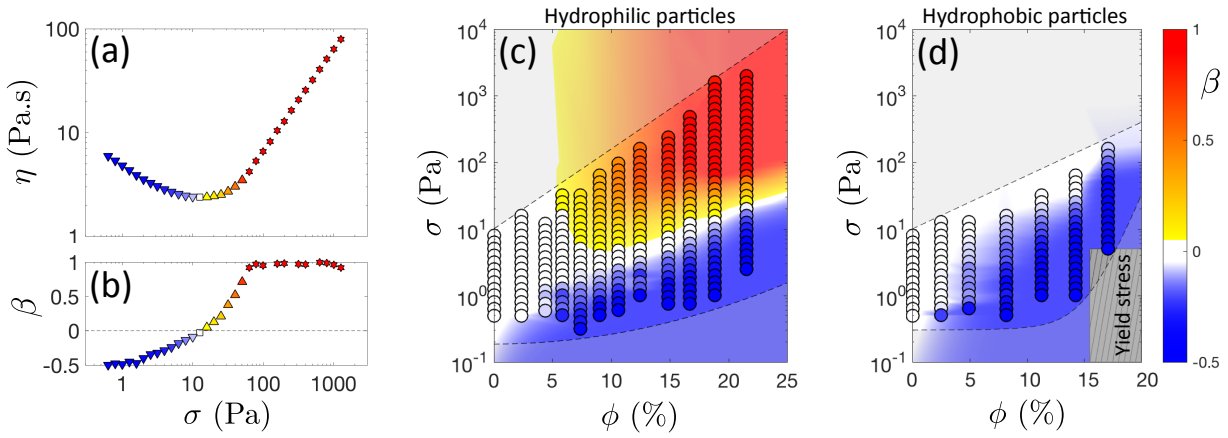

FIG. 2: (color online) (a) Viscosity η and (b) slope parameter $\beta = \dot{\gamma}(\mathrm{d}\eta/\mathrm{d}\sigma)$ vs shear stress σ for a suspension of hydrophilic fumed silica particles ($\phi = 18.9\%$, $R_\mathrm{u} = 25$ nm). Different regimes are defined with respect to β: shear thinning ($\beta < 0$, ▼), Newtonian ($\beta = 0$, □), CST ($0 \leq \beta < 1$, ▲) and DST ($\beta \to 1$, ⋆). (c) Phase diagram (σ, ϕ) for hydrophilic fumed silica particles. The hollow black circles represent individual steady-state rheological measurements and colors encode the values of β. We used the same color code as in (a) and (b). (d) Phase diagram (σ, ϕ) for hydrophobic fumed silica particles. Same color code as in (a)-(c). Suspensions of hydrophobic fumed silica do not exhibit any shear-thickening transition. The grey hatched rectangle at low stress and high volume fraction denotes the region influenced by the yield stress. In both (c) and (d), the two areas shaded in light grey transparency at low and high shear stress correspond to regions that cannot be accessed experimentally (see SI-6).

shear rates ($\dot{\gamma} < 20$ s^{-1}), whereas the viscosity begins to slowly increase at high shear rates, which is characteristic of CST [17, 37]. This trend is amplified for increasing volume fractions of fumed silica, up to $\phi = 16.7\%$ for which the viscosity jumps by an order of magnitude over a narrow range of shear rates. Finally, for even larger volume fractions ($\phi = 21.5\%$), an abrupt shear-thickening transition occurs at an almost constant critical shear rate of about 15 s^{-1}, which corresponds to DST [8, 13, 40]. In this suspension, the CST and DST transitions thus occur respectively at $\phi_\mathrm{CST} \simeq 5\%$ and $\phi_\mathrm{DST} \simeq 18\%$. Strikingly, these volume fractions are significantly lower than that reported in the literature, where shear thickening is usually observed for $\phi \gtrsim 50\%$ in the vicinity of the jamming point ϕ_J, in dense suspensions of both Brownian and non-Brownian particles with more regular shapes [2, 23, 25, 41] although the precise value for the transition is affected by the particle geometry [42]. This result suggests the presence of strong dynamic interactions between fumed silica particles at packing fractions much lower than the jamming fraction ϕ_J, which arise from the complex structural geometry of our particles. In a similar way, the fractal-like structure of carbon black particles leads to suspensions that exhibit weak shear thickening [43] or the appearance of a yield stress behavior at similar low volume fraction [44]. However, it is important to note that discontinuous shear thickening is not reported in carbon black suspensions. One important distinction is the hydrophobic nature of carbon black which typically necessitates the use of apolar organic solvents [45].

In order to directly probe the effect of the particle surface chemistry, we repeat the same rheological measurements on suspensions of *hydrophobic* fumed silica particles. These particles are coated with a nanometric layer of silanes. They display identical geometrical features (R_u, N_u and D) as the hydrophilic particles [see Fig. 1(d) and SI-1] but have different surface chemistry. As we show in Fig. 1(e), a surface coating of these particles on a glass slide results in a superhydrophobic surface with contact angle $\theta \geq 150°$. At low volume fraction, those hydrophobic particles still disperse in polypropylene glycol. As observed in Fig. 1(f), suspensions of hydrophobic fumed silica exhibit a strikingly different response from that observed with hydrophilic particles at the same volume fraction [Fig. 1(c)]. These hydrophobic particulate suspensions display a purely shear-thinning response over the entire range of volume fractions explored. The shear-thinning effect becomes more pronounced for increasing volume fractions, in part due to the gradual appearance of a yield stress at large volume fractions ($\phi \geq 17.1\%$, see SI-5). However, none of the suspensions of hydrophobic particles investigated show any shear-thickening behavior at high rates. This result shows that modifying the surface chemistry of the fumed silica particles from hydrophilic to hydrophobic has fully suppressed the shear-thickening transition over the entire range of shear rates 0.1 s$^{-1} \leq \dot{\gamma} \leq 100$ s^{-1} studied.

To further illustrate the difference between hydrophilic and hydrophobic fumed silica suspensions, and to quantify the shear-thickening magnitude, we introduce a dimensionless local parameter β defined as $\beta(\sigma) = \dot{\gamma}(\mathrm{d}\eta/\mathrm{d}\sigma) = \mathrm{dln}(\eta)/\mathrm{dln}(\sigma)$ which is directly associated

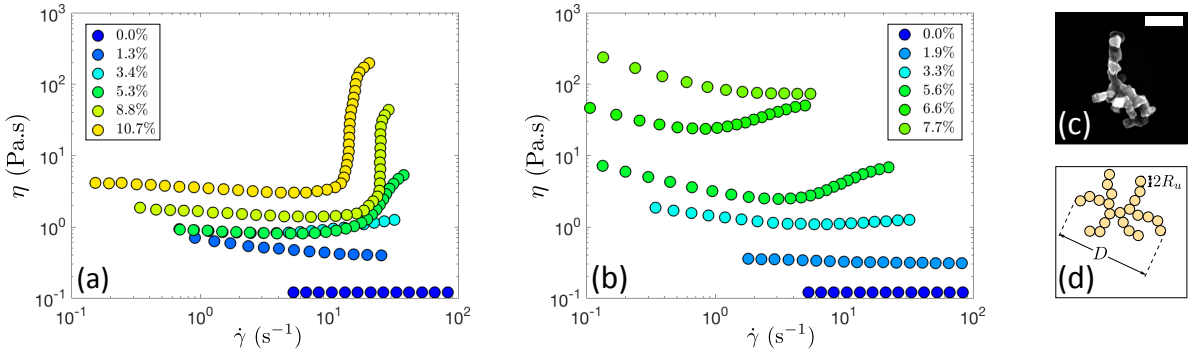

FIG. 3: (color online) Rheology of suspensions formulated from rough fumed silica particles. (a) Viscosity η of a suspension of hydrophilic fumed silica particles ($R_u = 10$ nm) vs the shear stress σ. The suspension exhibits shear thinning in the dilute regime (blue) before showing CST for $\phi = 3.4\%$ and 5.3% up to DST at a volume fraction of 8.8%. (b) Viscosity η of a suspension of rough hydrophobic fumed silica particles ($R_u = 10$ nm) vs the shear stress σ. The suspension exhibits moderate CST and develops a yield stress at high volume fraction. (c) SEM image of a representative hydrophobic particle composed of primary units of size $R_u = 10$ nm. The scale bar represents 150 nm. (d) Sketch depicting the geometry of these highly-textured fumed silica particles.

with the slope of the flow curve $\eta(\sigma)$ similarly to previous studies [37, 41]. By definition, $\beta = 0$ for a Newtonian fluid, whereas $\beta < 0$ ($\beta > 0$ resp.) for a shear-thinning (shear-thickening resp.) behavior. Finally, the parameter β saturates at $\beta = 1$, when the suspension goes through DST. The evolution of the suspension viscosity and β with shear stress is illustrated respectively in Fig. 2(a) and 2(b), for a suspension of hydrophilic fumed silica particles in PPG at $\phi = 18.9\%$. For increasing stress values, β smoothly varies from -0.5 to 1, which corresponds to a sequence of rheologically-distinct behaviors of the silica suspension from shear thinning (▼) to Newtonian (□), CST (▲) and finally DST (⋆). By repeating such analysis for the flow curves of all measured formulations (i.e., different volume fractions), a rheological state diagram of σ vs ϕ for the suspension of hydrophilic fumed silica particles with $R_u = 25$ nm is obtained as shown in Fig. 2(c). Black circles correspond to individual experimental data points, whilst colors encode the local value of $\beta(\phi,\sigma)$. Negative values scale from deep blue (pronounced shear thinning, $\beta = -0.5$) to light blue (weakly shear thinning, $\beta \to 0^-$), white values represent the Newtonian regime ($|\beta| < 0.05$), whilst the shear-thickening magnitude is represented by a continuous gradient from yellow ($\beta \sim 0.1$) to red ($\beta \to 1$). This phase diagram for suspensions of hydrophilic fumed silica clearly shows a combination of shear thinning at low shear stress and CST above a critical volume fraction ($\phi_{CST} \sim 5\%$). At larger volume fractions, DST appears for stresses larger than $\sigma_{DST} \simeq 30$ Pa.

The analogous phase diagram of σ vs ϕ for suspensions of hydrophobic fumed silica particles is illustrated in Fig. 2(d). In agreement with Fig. 1(b), $\beta < 0$ over the entire compositional range studied, which highlights the absence of any CST or DST up to $\phi = 20\%$. These results demonstrate the key role of the particle surface chemistry on the macroscopic rheology. Indeed, under strong shear, hydrophilic fumed silica particles can dynamically form inter-particle hydrogen bonds due to the presence of the hydroxyl groups at the surface of the particles [39, 46]. Hydrogen bonds have been previously reported to enhance shear thickening in dense suspensions [24, 33–35]. It is clear that coating hydrophilic particles with alkylsilane chains produces hydrophobic particles [Fig. 1(e)], and inhibits the creation of interparticle hydrogen bonds causing the complete extinction of the shear-thickening transition over this range of volume fraction.

Very recently James *et al.* have shown that particle geometry is also important in controlling the range of volume fractions for which shear thickening is observed [42]. To clarify the important contribution of particle surface roughness to the above picture, we have also performed another series of rheological experiments on rougher particles. These fumed silica particles are composed of a larger number of nodules ($N_u \simeq 150$) of smaller size $R_u \simeq 10$ nm corresponding to a markedly higher specific surface area (SI-1). However, these "rough" particles possess the same global size $D = 300$ nm as the smoother particles (with $R_u \simeq 25$ nm) studied in the first part of this article. As reported in figure 3(a), suspensions of these rough (high specific surface area) hydrophilic particles exhibit flow curves similar to that previously described for the smoother (lower specific area) fumed silica [Fig. 1(c)]. While only shear-thinning behavior is noticed in the dilute regime, CST now appears at $\phi_{CST} \simeq 3.4\%$ and DST now occurs for these highly-textured particles at a volume fraction as low as $\phi_{DST} \simeq 8.8\%$. These values are significantly lower than those reported for the smoother particles [Fig. 2(c)].

These rough fumed silica particles can also be made

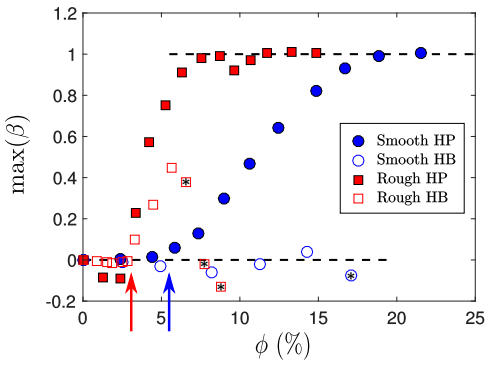

FIG. 4: (color online) Maximum value of β vs volume fraction ϕ determined for four different types of particles characterized by their texture $R_u = 10$ nm (rough particles, red squares) or 25 nm (smooth particles, blue circles), and their surface chemistry: hydrophilic (HP, filled symbols) or hydrophobic (HB, open symbols). shear thickening is observed for both types of rough particles ($R_u = 10$ nm) and only for hydrophilic smooth particles ($R_u = 25$ nm) above a critical volume fraction ϕ_{CST}, which depends on the geometry of the silica particles. Continuous shear thickening appears at $\phi_{CST} \simeq 3.4\%$ (resp. 5%) for $R_u = 10$ nm (resp. 25 nm). The onset of CST is marked by a red (resp. blue) arrow on the graph. Dashed horizontal lines mark the specific values 0 and 1 of max(β) defining onsets for CST and DST, respectively. The black stars within certain hollow symbols indicate the existence of a yield stress.

hydrophobic by silanization [Fig. 3(c)]. The corresponding rheology, illustrated in Fig. 3(b) for different volume fractions, shows strong similarity with the case of the smoother particles discussed in Fig. 1(f). The abrupt discontinuous shear-thickening transition observed for hydrophilic rough particles is spectacularly attenuated by the hydrophobic surface treatment. Nonetheless, these suspensions of rough hydrophobic particles still exhibit a weak and yet noticeable shear-thickening behavior at large shear rate. However, this CST is only observed over a narrow range of volume fractions $\phi_{CST} \simeq 3.4\% \leq \phi \leq 7\%$. Beyond this range of volume fractions, the shear thickening is swamped by the rapid rise in the low shear-rate viscosity (denoting the development of a strong thixotropic behavior and the presence of a yield stress) [see Fig. 3(b) and the corresponding phase diagram in SI-7]. The existence of a weak but measurable shear thickening for rough hydrophobic particles at moderate volume fraction demonstrates the possibility of generating some shear thickening even in the absence of attractive chemical forces. This has also been reported for other experimental systems [43], and recent simulations [12, 47]. However, local reversible chemical bonds such as interparticle hydrogen bonds enhance this phenomenon and are necessary to induce DST.

From these observations, it is clear that the DST observed in suspensions of hydrophilic rough particles reported in Fig. 3(a) arises from interparticle friction enhanced by reversible chemical interactions, which favor prolonged contact between the textured particles forced into close proximity under strong shear. For smoother particles, the interparticle friction is too weak to produce shear thickening by itself in the absence of additional short-range chemical interactions as reported in Fig. 1(b). At higher volume fractions, in the absence of a stabilizing solvation layer, these high surface area particles slowly assemble into a colloidal gel through long range hydrophobic interactions [48, 49] (see SI-5).

In summary, the differences in rheological behavior between the suspensions of particles with two different surface roughness and two different chemical philicities show that the microscopic mechanism for shear thickening is based on a synergy between solid friction and reversible hydrogen bonding; the former being the primary factor and the latter being crucial for discontinuous shear thickening at moderate volume fractions. Suspensions formulated from rough and smooth fumed silica particles also differ by the critical conditions required for the onset of CST and DST. These differences can be easily visualized by plotting the maximum of the slope parameter β as a function of the volume fraction ϕ. The results for the four distinct families of suspensions investigated in this article are represented in Fig. 4.

For suspensions of the rougher silica particles ($R_u = 10$ nm), CST is observed for volume fractions $\phi \geq \phi_{CST} \simeq 3.4\%$, regardless of whether they have hydrophilic or hydrophobic surface treatments, suggesting this shear-thickening transition is driven by frictional interactions between the highly roughened particles. By contrast, for smoother silica particles, CST is only observed for hydrophilic particles, for $\phi \geq \phi_{CST} \simeq 5\%$.

To understand the origin of these remarkably low values for ϕ_{CST} compared to that of other experimental systems reported in the literature, we define an inter-particle distance L by allocating a volume L^3 to each single particle of volume Ω_p such that $\phi \sim \Omega_p/L^3$. The volume Ω_p occupied by one particle is the sum of N_u quasi-spherical nodules each of size R_u that have been sintered together, which reads $\Omega_p \simeq N_u(4/3)\pi R_u^3$, the interparticle distance L thus scales as follows:

$$L \sim \left[\frac{4\pi N_u R_u^3}{3\phi}\right]^{1/3} \quad (1)$$

and decreases for increasing volume fractions of suspended solids. For our textured particles, frictional interaction will become important when the interparticle distance becomes comparable to the particle size, i.e., $L \simeq D$. This criterion defines the critical volume fraction ϕ_{CST} at which shear thickening begins, and depends only on the physical structure of the textured particles (via D, R_u and N_u). This estimate of the conditions for the onset of CST is identical for suspensions of rough particles with both hydrophilic and hydrophobic properties as also noted experimentally in Fig. 4 (see for example

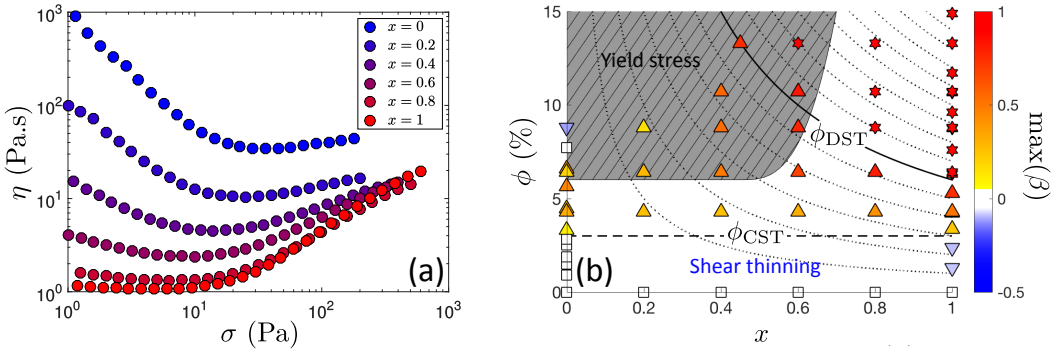

FIG. 5: (color online) Rheology of mixed suspensions of hydrophilic and hydrophobic silica particles. (a) Flow curves $\eta(\sigma)$ of mixed suspensions of fixed volume fraction $\phi = 6.4\%$ for different ratio x of hydrophilic to hydrophobic silica particles ($R_u = 10$ nm). The rheology shifts from DST for a suspension of pure hydrophilic particles ($x = 1$, •) to a moderate CST for a suspension only composed of hydrophobic particles ($x = 0$, •). (b) Phase diagram volume fraction ϕ vs hydrophilic ratio x for mixed suspensions of hydrophilic and hydrophobic silica particles. Colors encode the value of max(β) ranging between -0.5 and 1. We observe four different regimes: Newtonian (□), shear thinning (▼), CST (▲ and ▲) and DST (★). The top left corner of the diagram that is shaded in grey corresponds to suspensions that show a yield stress. Dotted lines represent iso-contour with a fixed number of hydrophilic particles. The solid line represents the onset of DST at $\phi_{DST}^{(HP)} = 6\%$.

□ and ■). Indeed, both types of particles display identical geometrical characteristics as they only differ by the monolayer silane coating (see SI-1).

Moreover, this geometric interpretation offers a quantitative estimate of ϕ_{CST}. We can estimate N_u from analysis of multiple SEM pictures (as displayed in SI-1), and find $N_u \simeq 150$ and $R_u = 10$ nm for the rough particles and $N_u \simeq 25$ and $R_u = 25$ nm for the smoother particles. By considering a constant size of particles ($D = 300$ nm), in good agreement with our SEM pictures, and using the scaling law described above, we can make an estimate of ϕ_{CST} that is in good agreement with the experimental results, i.e., $\phi_{CST}^{th} \simeq 3\%$ for $R_u = 10$ nm (vs $\phi_{CST} \simeq 3.4\%$) and $\phi_{CST}^{th} \simeq 6\%$ for $R_u = 25$ nm (vs $\phi_{CST} \simeq 5\%$). Despite its simplicity (and the incertitude on the value of N_u), this geometrical approach provides a simple scaling for the surprisingly low critical volume fraction required for obtaining shear thickening for these textured particles. Furthermore, the proposed criterion for CST being based on frictional contact between particles, our approach supports a mechanism involving solid friction amplified by short-range (< 1 nm) reversible physico-chemical interactions (such as hydrogen bonds) rather than a scenario based on hydrodynamic forces, which might be expected to dominate at long range (> 100 nm) [11, 50, 51]. Although moderate CST can be obtained in the absence of hydrogen bonds (□ in Fig. 4), it is fully suppressed in the range of volume fraction studied by reducing the nanometric roughness of the particles (○ in Fig. 4), a key factor to tune the solid friction. Regardless of the scale of the roughness, the presence of local hydrogen bond interactions is essential to achieve the extreme DST documented in Fig. 1(c), Fig. 2(c) and Fig. 3(a) ($\beta \to 1$).

Mixtures.- To offer some insights on the competitive effects of particles with opposite surface properties on the shear-thickening transition, we now dilute our suspensions of hydrophilic (HP) fumed silica by substituting some fraction of particles with hydrophobic (HB) fumed silica particles of identical geometrical features ($R_u = 10$ nm). The relative amount of hydrophilic to hydrophobic particles is quantified by the ratio $x = V_{HP}/(V_{HP} + V_{HB})$, where V_{HP} (resp. V_{HB}) denotes the volume of hydrophilic (resp. hydrophobic) particles such that $V_{HP} = N_{HP}\Omega_p$ with N_{HP} the number of hydrophilic particles. Figure 5(a) shows the viscosity of six suspensions of mixed HP and HB rough silica particles as a function of the shear stress σ at a given volume fraction fixed to $\phi = (V_{HP} + V_{HB})/V = 6.4\%$, with V the total volume of the suspension. At $\phi = 6.4\%$, the suspension of purely hydrophobic particles ($x = 0$) exhibits only a weak shear-thickening behavior, whereas the suspension of solely hydrophilic particles ($x = 1$) shows DST ($\beta = 1$) with $\eta \propto \sigma$, as already discussed in Fig. 3. The suspensions of intermediate compositions ($x = 0.2$, 0.4, 0.6, and 0.8) show a smooth variation of intermediate rheological response between the two pure limiting cases. In terms of shear thickening, the slope parameter β allows us to determine how the magnitude of shear thickening is shifted from DST to weak CST as we progressively substitute the attractive hydrophilic particles with hydrophobic ones (SI-8). By exploring systematically the effect of ϕ and x, we can construct the rheological state diagram reported in Fig. 5(b), which captures the various rheological regimes of these mixed compositions. For each formulation, the maximum value of the slope parameter, max(β), is reported as a function of ϕ and x. Using the same color scheme and symbols as in Fig. 2, we observe that low total volume fractions always lead to a

shear-thinning behavior (▼), which is more pronounced in the presence of hydrophilic particles. Above a critical volume fraction ($\phi_{CST} \simeq 3.4\%$), continuous shear thickening appears (▲ and ▲) for all compositions regardless of x; however, the magnitude of shear thickening increases with x in agreement with our previous observations. DST (⋆) is observed at larger volume fractions ($\phi > 12\%$) in the regime where most of the particles are hydrophilic ($x > 0.5$). Finally, for large volume fractions of hydrophobic particles ($\phi > 6\%$ and $x < 0.6$), long-range colloidal interactions between the dispersed particles result in a weak gel with a yield stress. This gives rise to a large shear-thinning viscosity that masks any shear-thickening contribution. This dynamic state diagram thus shows the rich variety of rheological regimes achievable by mixing different particle chemistries.

As recently described in the case of bi-disperse suspensions, exploring the rheological response of mixtures can also contribute to better understanding of the onset conditions for DST [52], which we might assert requires a critical number of interparticle frictional contacts. Under this assertion, DST is controlled by exceeding a critical volume fraction of hydrophilic particles $\phi_{DST}^{(HP)} = x\phi_{DST}$ [see thick solid line described by the expression $\phi_{DST} = 6/x$ in Fig. 5(b), where $\phi_{DST}^{(HP)} \simeq 6\%$ for pure hydrophilic particles ($x = 1$) with $R_u = 10$ nm]. Experiments above this compositional limit indeed show DST for $x \geq 0.8$. However, this is not the case for $x \leq 0.6$ for which we only observe a strong but continuous shear-thickening response at a volume fraction $\phi = 10.7\%$ slightly above the anticipated value of $\phi_{DST} = 6/0.6 = 10\%$. However, we do ultimately achieve DST at an even higher composition of $\phi = 13.3\%$. These results suggest that the incorporation of hydrophobic particles leads to an additional screening of the short-range chemical attractions between hydrophilic particles. This screening effect inhibits the strong sample-spanning frictional interactions required to achieve the DST state but can be overcome by further increasing the volume fraction of hydrophilic particles.

Conclusion.- Whilst some degree of shear thickening is often observed in dense suspensions, here we have shown that both CST and DST can be achieved at low volume fractions with hydrophilic fumed silica particles possessing high specific surface areas. The surface roughness of these geometrically-irregular particles appears as the primary control parameter to drive the onset of CST, in agreement with recent experimental and numerical results [13, 21, 24, 25, 41, 53]. Moreover, shear thickening occurs at low volume fractions and persists over a large range of volume fractions [from 5% to 23% in Fig. 2(c)] where the critical shear stress for shear thickening varies by over a decade [Fig. 2(c)]. However, we also show that DST is only observed in the presence of sufficient levels of hydrogen bonding between particles. More spectacularly, reducing the level of roughness and eliminating hydrophilic interactions result in the complete suppression of the shear-thickening regime. Finally, we have mapped out a rheological phase diagram for mixtures of hydrophilic and hydrophobic silica particles, which demonstrates the possibility to finely tune the rheological behavior of these fumed silica suspensions by blending hydrophilic and hydrophobic particles. In this way, we screen strong reversible interparticle interactions and systematically reduce the shear thickening, an observation of obvious practical interest in cement paste rheology [54]. This work paves the way for the design of cheaper and more stable shear-thickening fluids requiring lower volume fractions of particles, which is of critical importance for numerous applications such as shock-absorbing composites [55]. The optical transparency of these materials (due to the close refractive index match between the fumed silica and the PPG matrix phase) also allows in-situ flow visualization and may provide complementary insights on the suspension microstructure that develops during the shear-thickening transition.

The authors thank R.E. Cohen, F. Galindo-Rosales and S. Manneville for fruitful discussions, as well as the MIT-France and MIT-Portugal seed fund program for financial support.

[1] J. Stickel and R. Powell, Annu. Rev. Fluid Mech. **37**, 129 (2005).
[2] J. Mewis and N. J. Wagner, *Colloidal suspension rheology* (Cambridge University Press, Cambridge, England, 2011).
[3] I. Cohen, T. G. Mason, and D. A. Weitz, Phys. Rev. Lett. **93**, 046001 (2004).
[4] X. Cheng, X. Xub, S. A. Rice, A. R. Dinner, and I. Cohen, Proc. Natl. Acad. Sci. USA **109**, 63 (2012).
[5] A. Vázquez-Quesada, R. I. Tanner, and M. Ellero, Phys. Rev. Lett. (2016).
[6] Z. Varga, V. Grenard, S. Pecorario, N. Taberlet, V. Dolique, S. Manneville, T. Divoux, G. H. McKinley, and J. W. Swan, Proc. Natl. Acad. Sci. USA **116**, 12193 (2019).
[7] D. Bonn, M. M. Denn, L. Berthier, T. Divoux, and S. Manneville, Rev. Mod. Phys. **89** (2017).
[8] H. A. Barnes, J. Rheol. **33**, 329 (1989).
[9] N. J. Wagner and J. F. Brady, Phys. Today **62**, 27 (2009).
[10] M. M. Denn, J. F. Morris, and D. Bonn, Soft Matter **14**, 170 (2018).
[11] G. Bossis and J. F. Brady, J. Chem. Phys. **91**, 1866 (1989).
[12] S. Jamali and J. F. Brady, Phys. Rev. Lett. **123**, 138002 (2019).
[13] R. Seto, R. Mari, J. F. Morris, and M. M. Denn, Phys. Rev. Lett. **111**, 218301 (2013).
[14] A. Liu and S. R. Nagel, Annu. Rev. Condens. Matter Phys. **1**, 347 (2010).
[15] M. Wyart and M. E. Cates, Phys. Rev. Lett. **112**, 098302 (2014).

[16] R. Mari, R. Seto, J. F. Morris, and M. M. Denn, JoR **58**, 1693 (2014).
[17] J. F. Brady and G. Bossis, J. Fluid Mech. **155**, 105 (1985).
[18] J. Bender and N. J. Wagner, J. Rheol. **40**, 899 (1996).
[19] J. R. Melrose and R. C. Ball, J. Rheol. **48**, 961 (2004).
[20] R. G. Egres and N. J. Wagner, J. Rheol. **49**, 719 (2005).
[21] N. Fernandez, R. Mani, D. Rinaldi, D. Kadau, M. Mosquet, H. Lombois-Burger, J. Cayer-Barrioz, H. J. Herrmann, N. D. Spencer, and L. Isa, Phys. Rev. Lett. **111**, 108301 (2013).
[22] F. Boyer, E. Guazzelli, and O. Pouliquen, Phys. Rev. Lett. **107**, 188301 (2011).
[23] Z. Pan, B. W. H. de Cagny, and D. Bonn, Phys. Rev. E **92**, 032202 (2015).
[24] J. Comtet, G. Chatté, A. Niguès, L. Bocquet, A. Siria, and A. Colin, Nature Com. **8**, 15633 (2017).
[25] C. Clavaud, A. Bérut, B. Metzger, and Y. Forterre, Proc. Natl. Acad. Sci. USA **114**, 5147 (2017).
[26] C. P. Hsu, S. N. Ramakrishna, M. Zanini, N. D. Spencer, and L. Isa, Proc. Natl. Acad. Sci. USA **115**, 5117 (2018).
[27] J. F. Morris, Phys. Rev. Fluids **3**, 110508 (2018).
[28] I. R. Peters, S. Majumdar, and H. M. Jaeger, Nature **532**, 215 (2016).
[29] B. Saint-Michel, T. Gibaud, and S. Manneville, Phys. Rev. X **8**, 031006 (2018).
[30] N. Park, V. Rathee, D. L. Blair, and J. C. Conrad, Phys. Rev. Lett. **122**, 228003 (2019).
[31] V. Gopalakrishnan and C. F. Zukoski, J. Rheol. **48**, 1321 (2004).
[32] E. Brown, N. A. Forman, C. S. Orellana, H. Zhang, B. W. Maynor, D. E. Betts, J. M. DeSimone, and H. M. Jaeger, Nature Materials **9**, 220 (2010).
[33] N. M. James, E. Han, R. Arturo, L. de al Cruz, J. Jureller, and H. M. Jaeger, Nat. Mater. **17**, 965 (2018).
[34] N. M. James, C.-P. Hsu, N. D. Spencer, H. M. Jaeger, and L. Isa, J. Phys. Chem. Lett. **10**, 1663 (2019).
[35] H. S. Son, K. H. Kim, J. H. Song, W. Lee, J. H. Kim, K. H. Yoon, Y. S. Lee, and H.-J. Paik, Colloid Polym. Sci. **297**, 95 (2019).
[36] D. Lootens, H. V. Damme, and P. Hébraud, Phys. Rev. Lett. **90**, 178301 (2003).
[37] E. Brown and H. M. Jaeger, Phys. Rev. Lett. **103**, 086001 (2009).
[38] H. Barthel, M. Heineman, M. Stintz, and B. Wessely, Chem. Eng. Technol. **21**, 745 (1998).
[39] S. R. Raghavan and S. A. Khan, J. Colloid Interface Sci. **185**, 57 (1997).
[40] E. Brown and H. M. Jaeger, J. Rheol. **56**, 875 (2012).
[41] J. R. Royer, D. L. Blair, and S. D. Hudson, Phys. Rev. Lett. **116**, 188301 (2016).
[42] N. M. James, H. Xue, M. Goyal, and H. M. Jaeger, Soft Matter **15**, 3649 (2019).
[43] C. O. Osuji, C. Kim, and D. A. Weitz, Phys. Rev. E **77**, 060402(R) (2008).
[44] J. J. Richards, J. B. Hipp, J. K. Riley, N. J. Wagner, and P. D. Butler, Langmuir **33**, 12260 (2017).
[45] M. van der Waarden, J. Colloid Sci. **5**, 317 (1950).
[46] S. R. Raghavan, H. J. Walls, and S. A. Khan, Langmuir **16**, 7920 (2000).
[47] A. Singh, R. Mari, M. Denn, and J. Morris, J. Rheol. **62**, 457 (2018).
[48] J. N. Israelachvili and R. Pashley, J. Colloid Interface Sci. **98**, 500 (1984).
[49] E. Meyer, K. Rosenberg, and J. Israelachivili, Proc. Natl. Acad. Sci. USA **103**, 15739 (2006).
[50] D. P. Kalman and N. J. Wagner, Rheol Acta **48**, 897 (2009).
[51] X. Cheng, J. H. McCoy, J. N. Israelachvili, and I. Cohen, Science **333**, 1276 (2011).
[52] Y. Madraki, G. Ovarlez, and S. Hormozi, Phys. Rev. Lett. **121**, 108001 (2018).
[53] N. Y. C. Lin, B. M. Guy, M. Hermes, C. Ness, J. Sun, W. C. K. Poon, and I. Cohen, Phys. Rev. Lett. **115**, 228304 (2015).
[54] F. Toussaint, C. Roy, and P. Jézéquel, Rheol. Acta **48**, 883 (2009).
[55] Y. Lee, E. Wetzel, and N. Wagner, J. Mater. Sci. **38**, 2825 (2003).